Study on the influence of TBM disc cutter on the penetration of extremely hard rock in Zijing Tunnel

Chao Gao[a], Yufeng Huang[b], Qi Geng[b*], Xiaowu Han[a], Huijian Zhang[c], Rucheng Hu[a], Fei Liu[a]

[a] The Electricity Engineering CO., LTD under CREC NO.5 Group, Changsha, Hunan 410000, China.
[b] School of Construction Machinery, Chang'an University, Xi'an, Shanxi 710064, China.
[c] School of Civil Engineering, Southwest Jiaotong University, Chengdu, Sichuan 610031, China.
*Corresponding author: gengqi@chd.edu.cn

Abstract

The reasonable setting of TBM disc cutter penetration depth is crucial for its rock-breaking efficiency in extremely hard rock geology. In the construction section of the Dujiangyan to Mount Siguniang Zijing Tunnel project, which encountered extremely hard diorite rock (with uniaxial compressive strength exceeding 230 MPa), to reveal the influence of penetration depth on disc cutter cutting of extremely hard diorite rock, the following steps were taken: Firstly, using a self-developed small-scale disc cutter linear rock-breaking test platform, experiments were conducted for four penetration depths: 1.5, 2.0, 2.5, and 3.0 mm, under fixed cutter spacing and with/without confinement conditions. Secondly, employing a high-precision crystalline rock material modeling method based on three-dimensional particle clusters, a full-scale numerical model of disc cutter linear cutting of diorite rock was established. Seven penetration depths ranging from 1.0 to 10.0 mm were tested under a fixed cutter spacing of 80 mm. Results indicate that under lateral confinement, diorite failure shifts from slip and extrusion to crushing, while under no confinement, it primarily spalls laterally with increased rock debris and ejection distance as penetration increases. The disc cutter normal force rises with penetration, with a critical 4mm point after which load increases slowly but penetration significantly, marking an efficient rock breaking stage. Specific energy efficiency peaks at 3mm penetration in tests and 4mm in simulations, attributed to test bench limitations. Combined results suggest an optimal penetration of 4mm.

Keywords

Full-face rock tunnel boring machine, Diorite, Disc cutter, Penetration depth, Discrete element

1. Introduction

With the rapid development of modern underground engineering technology, the full-face rock tunnel boring machine (TBM) has become widely utilized as efficient excavation equipment in tunnel construction across various geological conditions. During TBM construction, the disc-shaped cutters on the cutterhead are driven by the driving device to penetrate the rock under the action of strong thrust and torque. As the penetration depth of the cutters increases, fragments are generated on the surface of the rock, and cracks form inside the rock. Under the interaction between adjacent cutters, these cracks extend and connect with each other, forming rock chips, thereby achieving the purpose of excavation. Penetration depth and cutter spacing are key factors affecting the rock-breaking efficiency of TBM cutters (Fu 2024).

The current research methods for studying the rock-breaking efficiency of TBM cutters primarily encompass on-site tests, laboratory experiments, and numerical simulations. A synthesis of notable studies is outlined in Table 1. Laboratory rock-breaking tests with TBM cutters enable the cutting of substantial rock volumes by regulating cutter spacing and penetration depth, thus mitigating the impact of size effect on rock-breaking efficacy. The resultant test data can be directly applied to engineering applications and facilitate the determination of TBM design parameters (Rostami et al. 1996). Gong et al. (2015; 2016) conducted linear cutting tests on Beishan granite, varying penetration depth from 0.5 to 3.5 mm via a mechanical rock-breaking test platform. Their research explored the impact of different penetration depths on rock-breaking efficiency, revealing that beyond a certain threshold, increasing penetration depth did not notably enhance rock-breaking efficiency. Snowdon et al. (1982) executed laboratory TBM cutter rock-breaking experiments across four distinct rock types. They scrutinized the influence of cutter spacing and penetration depth on single-cutter rock-breaking loads and specific energy. Their findings indicated that the ratio of cutter spacing to penetration depth, corresponding to minimum specific energy, remained consistent across different rocks, with uniaxial compressive strength significantly affecting rock-breaking effectiveness. Moreover, specific energy diminished gradually with rising penetration depth, plateauing beyond a critical value. Gertsch et al. (2007) conducted TBM cutter rock-breaking experiments on granite, exploring various penetration depths and cutter spacings. They determined an optimal cutter spacing of 76 mm, minimizing the impact of penetration depth on specific energy at this spacing. Cho et al. (2013) ascertained optimal

conditions for cutting Korean granite with TBM cutters via full-scale linear cutting tests and 3D measurement technology. By comparing results with numerical simulations, they validated the applicability of numerical calculation methods for predicting cutter penetration behavior. Tan et al. (2010; 2012a; 2012b) developed a two-dimensional TBM cutter cutting model using the discrete element method (DEM), simulating the effects of different confining pressures, cutter spacings, and cutting sequences on TBM cutter rock-breaking efficiency. Kou et al. (1999) and Liu et al. (2002) simulated rock crack propagation under TBM cutter action using finite element software RFPA2D. Su et al. (2009) simulated TBM cutter rock-breaking using the discrete element method, demonstrating that under equivalent penetration depth, the cutter's rock-breaking ability increased with a higher cutter ring rake angle and cutter count. Wang et al. (2014) investigated the influence of penetration depth, cutting speed, and cutter spacing on TBM cutter rock-breaking performance through full-scale rock-breaking tests, concluding that increased penetration depth and cutting speed correlated with higher rock-breaking force. Cheng (2017) employed a nonlinear elastoplastic constitutive model to numerically simulate the rock-cutting process of double TBM cutters, verified through double TBM cutter rock-breaking tests on a rotary cutting platform, and explored optimal penetration depth under specific rock conditions. Geng et al. (2022a; 2022b) utilized the combined ABAQUS-SPH method to simulate the rock-cutting process of double TBM cutters and analyzed the influence of cutter spacing on cutting efficiency.

For specific engineering projects, TBM cutters and cutters spacing are typically fixed and not easily adjustable. Achieving optimal rock-breaking efficiency necessitates dynamic adjustments to the thrust of hydraulic cylinders and the cutterhead rotation speed according to the rock conditions to match the optimal penetration depth. Existing studies mostly report uniaxial compressive strengths of rocks below 200 MPa, with limited research on TBM cutter performance on higher-strength extremely hard rocks. In this study, based on the Zijing Tunnel project of the Dusi Mountain urban rail transit, with a tunnel diameter of 10.23 m and extremely hard diorite with a uniaxial compressive strength of 234.6 MPa, we employ a research method combining laboratory straight-line cutting tests with discrete element simulation of particle clusters to investigate the variation in TBM cutter rock-breaking efficiency with penetration depth. We determine the optimal penetration depth for TBM

Author	Research method	Rock type and uniaxial compressive strength
Gong et al. (2015; 2016)	LCM	North Mountain granite，105.6MPa
Snowdon et al. (1982)	In situ excavation test and LCM	Sandstone, limestone, diabase, and granite，50-340MPa
Gertsch et al. (2007)	LCM	Coarse-grained red granite，158MPa
Cho et al. (2013)	LCM and 3D numerical analysis	Korean granite，209MPa
Tan et al. (2010)	DEM^{2D} and LCM	sandstone，12.7MPa，uniaxial tensile strength
Tan et al. (2012a; 2012b)	DEM^{2D} and RCM	Homemade cement mortar specimens，21.88MPa
Kou et al. (1999; 2002)	RFPA^{2D}	
Su et al. (2009)	PFC^{2D} and RCM	Rock specimens，47-200MPa
Wang et al. (2014)	LCM	Granite，146MPa
Cheng (2017)	D−P constitutive model and RCM	Rock specimens，21.88MPa
Geng et al. (2022a; 2022b)	RCM and ABAQUS-SPH coupling	Homemade concrete specimens，42.1MPa

Note: LCM is an indoor full-scale linear rock-breaking test, and RCM is an indoor full-scale rotary rock-breaking test.

cutter cutting extremely hard diorite, providing a theoretical basis for setting on-site excavation parameters.

2. Introduction to the Zijing Tunnel project of the D-S projects

The Zijing Tunnel of the Dusi Mountain urban rail transit project spans a total length of 10,411.18 meters, featuring a single-bore double-track design. The tunnel comprises one cross passage (located at DK35+880, with a length of 238 meters) and one inclined shaft (serving as both a ventilation and refuge area, positioned at DK42+850, with a length of 355 meters). The construction method primarily employs TBM excavation combined with conventional mining methods. The tunnel section from the entrance to DK36+230 is constructed using conventional mining methods (drill and blast), while the sections from DK36+230 to DK42+360 and from DK42+885 to DK44+980, totaling 8,225 meters, are constructed using TBM. Other sections are constructed using conventional mining methods (non-blasting). This study specifically focuses on the TBM construction section. The geological conditions of the main tunnel primarily comprise diorite and diorite gneiss, with a maximum compressive strength exceeding 250 MPa. The tunnel intersects eight fault zones with abundant water, with a maximum burial depth of 709 meters and a risk of high-stress rock bursts. The excavation employs the "Shutong" open-type TBM, independently developed by China Railway Engineering Equipment Group Co., Ltd. The cutterhead diameter is 10.23 meters, utilizing a "4+2" segmented manufacturing scheme. It is equipped with 4 double-disk center cutters with a diameter of 432 mm, 46 main cutters, and 12 edge cutters, all with a diameter of 483 mm. The average spacing between cutters is 80 mm.

Conducting excavation tests at various penetration depths poses challenges and is costly due to on-site testing constraints. Therefore, this study utilizes a self-developed small-scale TBM cutter linear rock-breaking test bench combined with discrete element numerical simulation technology for comprehensive scientific research. By employing the discrete element model of particle clusters, we successfully replicate the physical and linear cutting experiments of the target rock samples, fully validating the effectiveness and scientific nature of this method. Furthermore, by combining the discrete element model of particle clusters with linear cutting experiments, we conducted a detailed investigation into the rock-breaking efficiency of TBM cutters under different penetration depth conditions. These research findings not only provide a theoretical foundation for optimizing the rock-breaking efficiency of TBM cutters but also offer valuable references for the design and construction of similar future projects.

3. Disc cutter linear rock-breaking test

3.1 Preparation of rock tests and testing of mechanical properties

The extremely hard diorite samples were obtained from sections DK37+000 to DK37+400, located near the tunnel bottom around the shield shoes after excavation. Core samples of the original rock were collected using a core drilling rig and subsequently transported to a specialized laboratory for cutting and polishing. Following the guidelines outlined in the "Engineering Rock Mass Test Methods Standard", rock mechanical property testing experiments were conducted using the RTR-1000 rock mechanics testing system at the Key Laboratory of Transportation Tunnel Engineering of the Ministry of Education, Southwest Jiaotong University. The loading process of the experiments and the failure morphology of the rock samples are depicted in Figure 1.

The uniaxial compression test samples generally displayed longitudinal fractures, whereas the Brazilian splitting test samples exhibited central splitting. The stress-strain curve is depicted in Figure 2. The initial segment of the curve is relatively flat, with no noticeable concave phenomenon, indicating the diorite's initial loading stage is relatively dense (Zhang et al. 2023). The post-peak segment of the curve exhibits a certain vertical drop and even a back-bending phenomenon, indicating strong brittleness (Tarasov et al. 2013). The average mechanical property parameters of the diorite are outlined in Table 2, with the uniaxial compressive strength measured at 234.6 MPa. According to the rock strength classification standards proposed by Xia et al. (2018) for TBM engineering rocks, this value exceeds the threshold for extremely hard rocks (uniaxial compressive strength greater than 160 MPa). Detailed mechanical parameters of the test rock samples are provided in Table 2.
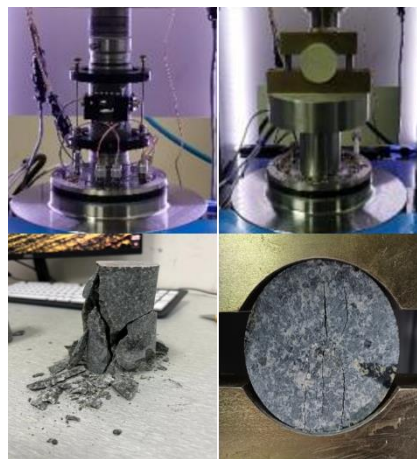

**Fig. 1 Granodiorite failure experiment and mechanical form**

Table 2. Rock sample physical-mechanical parameters (average values)

| Rock type	Poisson's ratio	Elastic modulus /GPa	Tensile strength /MPa	Compressive strength	Density /(kg/m³)
Diorite	0.3	40.0	21.0	234.6	3000

3.2 Disc cutter rock-breaking test design

Disc cutter rock-breaking test bench and specimens

To explore the influence of TBM cutter penetration depth on rock-breaking load and efficiency, a small-scale TBM cutter linear rock-breaking test bench, independently developed by the Key Laboratory of Road Construction Technology and Equipment of the Ministry of Education at Chang'an University, was utilized. The test bench, depicted in Figure 3, was employed to conduct linear rolling cuttings on the diorite samples. The experimental platform primarily comprises three core components: the driving system, the test bench body, and the testing system. It can accommodate rock samples with maximum dimensions of 500 mm in length, 200 mm in width, and 100 mm in height. To ensure the accuracy and reliability of the experiments, ultra-thin hydraulic jacks with capacities of 50 tons and 100 tons were arranged laterally and longitudinally. These jacks not only provide the necessary constraints to simulate a real rock fracturing environment but also, due to their ultra-thin design, minimize the occupation of experimental space, ensuring the flexibility and efficiency of the experimental process. For clamping the rock samples and applying confining pressure, an SWL series hand-operated screw jack device was specially installed above the rock box. This
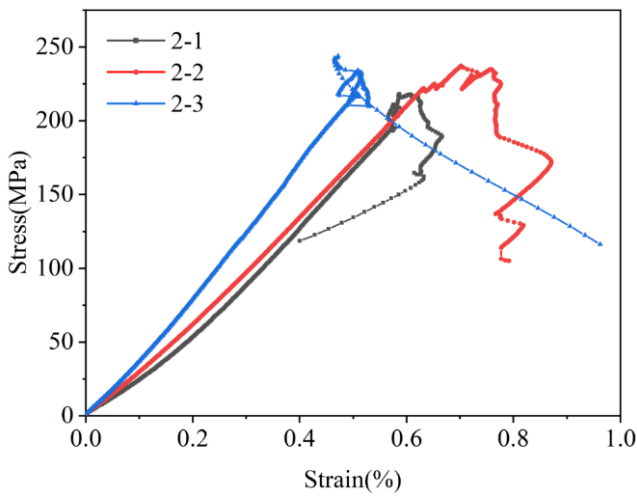
(a) Uniaxial compression test stress-strain curves
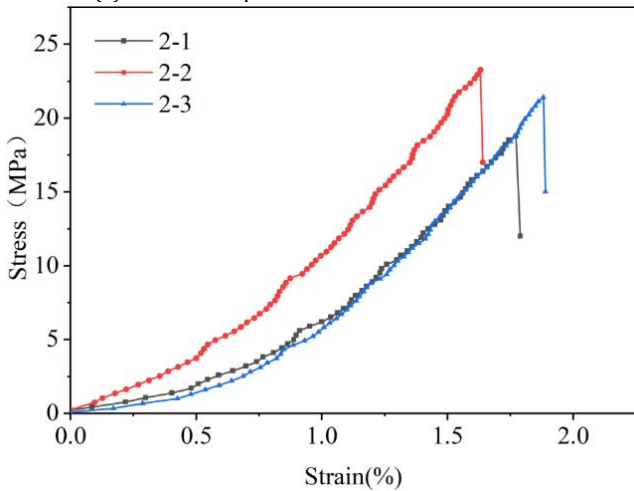
(b) Stress-strain curves for the Brazilian splitting test

Fig. 2 Stress-strain curve for rock sample in physical mechanics' experiment

device can effectively resist the reaction force of the TBM cutter rock-breaking, ensuring the longitudinal stiffness of the tool module. By manually rotating the screw, the penetration depth of the cutter can be precisely set. The rock box is driven along the longitudinal direction by a motor-screw drive system. This precise movement control allows the rock samples to have effective relative rolling with the cutter, thus smoothly completing the cutting and rock-breaking action of the cutter. To ensure the accuracy and reliability of the experimental data, three-axis force sensors were utilized to monitor and record the normal force, rolling force, and lateral force during the TBM cutter rock-breaking process in real time. The sampling frequency of the sensors was 100 Hz, with a range of 0~50 kN and a sampling accuracy of 1 N. At the tunnel site, core samples of diorite with an inner diameter of 200 mm were obtained using a core drilling rig. These samples were then cut into rectangular specimens with dimensions of 250 mm in length, 150 mm in width, and 100 mm in height. Surface polishing was conducted to ensure the flatness and parallelism of the sample surfaces, thus preventing errors in actual penetration depth caused by uneven samples. The prepared samples are depicted in Figure 3.

Fig. 3 Small-scale disc cutter linear rock-breaking test bench

Disc cutter rock-breaking test scheme

To closely simulate the TBM cutter rock-breaking process, the 483 mm diameter standard cross-section cutter used at the Zijing Tunnel site was scaled down to a 43.2 mm diameter cutter with a blade width of 1.7 mm at a ratio of 1:11.2. Referring to the actual TBM's average cutter spacing of 80 mm, the cutter spacing for indoor rock-breaking tests was set to 9 mm, approximately scaled down at a ratio of 1:11.2. The cutting line speed of the fixed cutter was set to 2.8 mm/s. Converted to a sampling frequency of 100 Hz, each adjacent load data point corresponds to a cutting distance of 0.028 mm, sufficient to reflect detailed load information during the TBM cutter rock-breaking process. Rock-breaking tests were conducted with cutter penetration depths of 1.5 mm, 2.0 mm, 2.5 mm, and 3.0 mm. To replicate real-world cutter cutting conditions as closely as possible, pre-cutting tests were conducted with a penetration depth set to 1 mm along the established cutting trajectory. Referring to previous full-scale TBM cutter linear rock-breaking tests (Li et al. 2022; Ji et al. 2023), it was observed that when the TBM cutter group first contacts the rock surface for 1~2 rotations, the rock under the cutter may not be completely broken. At this stage, due to the lack of effective voids between adjacent cutters, the rock-breaking of the cutter mainly exhibits a single-cutter rock-breaking mode with lateral constraints, defined as the "constrained mode". As the TBM enters a stable excavation state, the cutter transitions into a continuous rotary penetration mode. At this point, the adjacent cutting marks provide small voids for a single cutter, thus removing lateral constraints to some extent, termed the "unconstrained mode". Therefore, to align the test results more closely with actual operating conditions, a combined constrained and unconstrained approach was employed in this experiment. Under each penetration depth, 5 constrained tests and 4 unconstrained tests were conducted to ensure the repeatability of the test results. In the constrained tests, the cutter spacing was set to 18 mm, while the unconstrained tests were conducted between the cutting marks of the 5 constrained tests. The test plan is illustrated in Figure 4. Five sets of constrained cutting tests were conducted initially, followed by four sets of unconstrained cutting tests. After each set of tests, the rock-cutting results, three-axis cutter forces, and rock chip mass data were recorded.
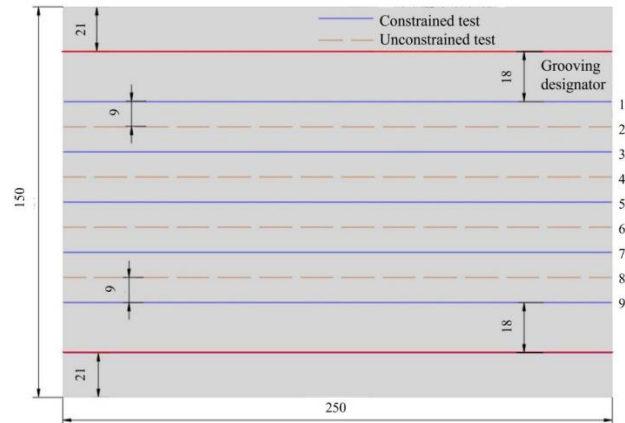

Fig. 4 Small-scale disc cutter linear rock-breaking test scheme

3.3 Analysis of the rock-breaking test results of the disc cutter

Rock-breaking effect and ballast quality

When the cutter penetration depth is 1.5 mm, the crushing action of the cutter on the rock is relatively minimal, resulting in the rock being crushed into a powdery state without forming obvious rock chips. In this scenario, rock damage primarily occurs due to the squeezing action of the cutter rather than the shearing action. This could be attributed to the constrained conditions that limit the lateral movement of the rock, thereby preventing it from releasing energy through shear.

When the penetration depth increases to 2 mm, a significant change in rock damage occurs under the unconstrained mode. At this stage, the rock surface damage becomes more severe, with many rock chips being crushed out. This indicates a transition in rock damage from simple squeezing to a combination of shearing and squeezing. This change is likely due to the increased penetration depth, which concentrates stress within the rock. Additionally, the small voids formed by cutting under constrained conditions partially remove lateral constraints, making it easier for the rock to fracture along shear planes.

When the cutter penetration depth reaches 2.5 mm and 3 mm, irrespective of whether under constrained or unconstrained conditions, rock crushing enters a new stage. Most rocks are crushed by the cutter into large rock chips. Upon clearing the rock chips, further observation of the rock surfaces between the cuttings reveals a more complete spalling phenomenon. This indicates that the increase in penetration depth contributes to improving the efficiency and integrity of rock crushing.
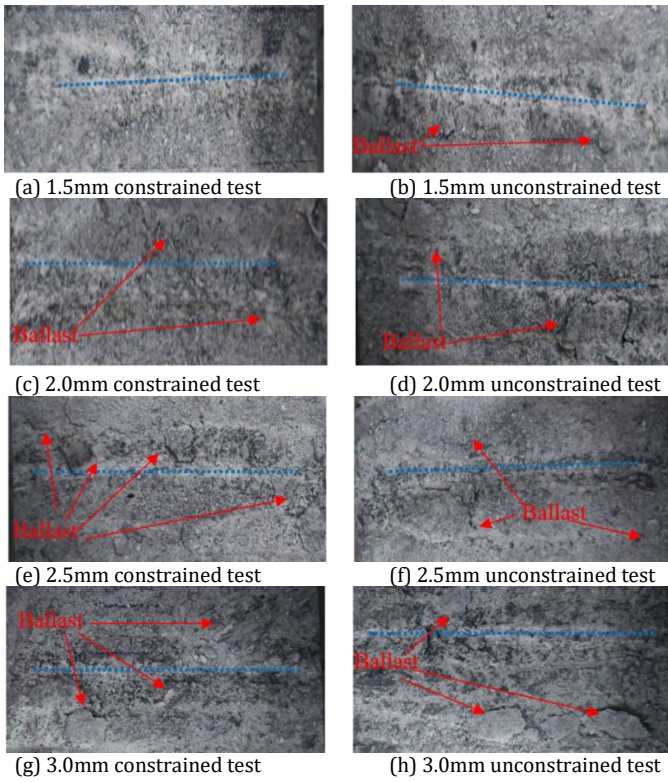
Fig. 5 Rock crushing state under different conditions of penetration depths

(a) 1.5mm constrained test
(b) 1.5mm unconstrained test
(c) 2.0mm constrained test
(d) 2.0mm unconstrained test
(e) 2.5mm constrained test
(f) 2.5mm unconstrained test
(g) 3.0mm constrained test
(h) 3.0mm unconstrained test

The collected and organized data regarding the mass of rock chips generated under different test conditions are presented in Figure 6. Under the penetration conditions of 1.5 mm, 2 mm, 2.5 mm, and 3 mm, the average mass of rock chips produced is 0.45 g, 1.5 g, 1.9 g, and 3 g, respectively. The average mass of rock chips increases with the increase in penetration depth.
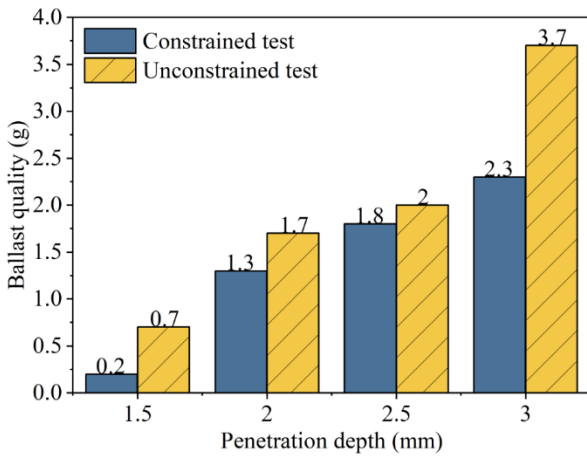

Fig. 6 The quality of ballast under different conditions of penetration depths

Comparing the mass of rock chips under two different boundary conditions reveals a clear trend: as the cutter penetration depth increases, the number of rock chips produced under unconstrained conditions gradually increases. This phenomenon indicates that under the unconstrained mode, the rock undergoes a more intense crushing action, resulting in more rock chips. In contrast, the mass of rock chips under the constrained mode is relatively smaller. This result suggests that under constrained conditions, due to the preset 9 mm cutter spacing, the rock crushing is somewhat restricted, resulting in ineffective interconnected destruction between the rocks within the cutter spacing.

Rock-breaking load and rock-breaking efficiency

The average normal force under different penetration depths is compared and calculated by the ratio of the area enclosed by the force-time curve and the length of the base. The analysis of the experimental results is presented in Figure 7. When the penetration depth is 1.5 mm, the average normal force in the constrained test is smaller than that in the unconstrained test. However, the difference in average normal force between the two constraint modes is not significant. At this relatively low penetration depth, the contact area between the cutter and the rock is small, and the extent of crack propagation and rock crushing inside the

rock is limited. Due to insufficient interconnection between the cutters, the promoting effect of the small voids formed under constrained cutting conditions on the rock-breaking effect of the cutter under the unconstrained mode is limited. Therefore, the average normal force under both modes is relatively small. When the penetration depth increases to 2 mm and 2.5 mm, the average normal force recorded in the constrained test exceeds that in the unconstrained test. This is because at this point, the interconnection between the cutters for rock breaking under constrained mode is more sufficient, and the cutting marks left by the constrained mode form voids, which helps to reduce the lateral constraint force. When the penetration depth is 3 mm, the average normal force in the constrained test is smaller than that in the unconstrained test again. The trend of the average rolling force and the average normal force is consistent, both increasing with the increase in penetration depth. When the penetration depth reaches 1.5 mm, the recorded average normal force is the smallest. As the penetration depth increases to 2 mm and 2.5 mm, the difference in average normal force between the constrained and unconstrained tests is not significant. This indicates that under the condition of a preset cutter spacing of 9 mm when the penetration depth is around 2 mm, the rock begins to enter an efficient crushing stage. Above this critical value, even if the penetration depth continues to increase, although the extent of rock fragmentation and the fluctuation amplitude of the load may become more severe, the rate of increase in the average load borne by the cutter begins to slow down.
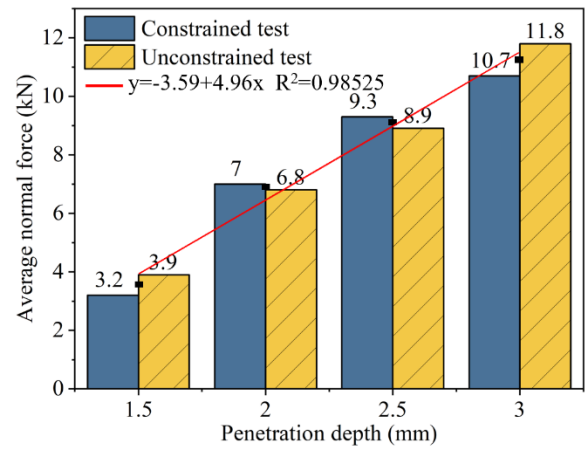

Fig. 7 Average normal force of disc cutter at different penetration depths

The specific energy under different penetration depths is shown in Figure 8. When the penetration depth is 1.5 mm, the specific energy of rock breaking in the unconstrained test is significantly lower than that in the constrained test.
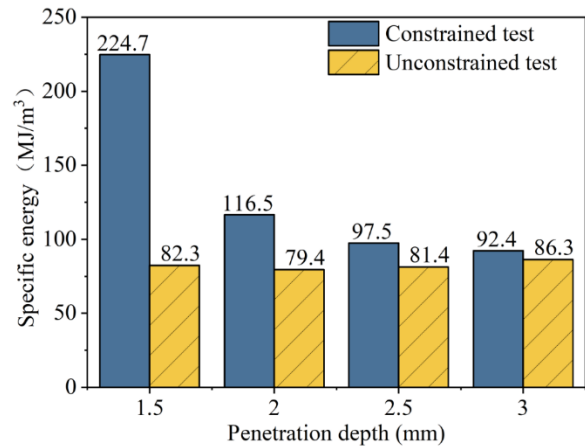

Fig. 8 Specific energy at different penetration depths

This is because the average rolling force under both constraint modes does not differ much. Under constrained conditions, the rock-breaking action of the cutter on the rock is relatively small, and the rock is crushed into a powdery state without forming obvious rock chips.

Under unconstrained conditions, the small voids formed by cutting under constrained conditions remove the lateral constraints to some extent, making rock fragmentation easier. Therefore, the specific energy of rock breaking in the unconstrained test is significantly lower than that in the constrained test.

When the penetration depth of the cutter further increases to 3 mm, under constrained conditions, there is a significant decrease in the specific energy required for rock breaking. This phenomenon occurs because

although the increase in average load is relatively small, there is a significant increase in the number of rock chips produced, indicating that the cracks under the cutter have started to connect, and the rock breaking is more complete, thus improving the energy utilization efficiency.

The specific energy of rock breaking under unconstrained conditions does not change much, and the specific energy of rock breaking under both boundary conditions is close in this range. The specific energy of rock breaking under constrained conditions is slightly higher than that under unconstrained conditions, indicating that under unconstrained conditions, the same rock breaking effect can be achieved with relatively less energy input, thereby improving the overall rock breaking efficiency.

4. Numerical simulation of rock-breaking by 3D disc cutter based on particle clusters

4.1 Mesoscopic parameter calibration of rocks based on particle clusters

The Discrete Element Method (DEM) offers an approach to explain the damage and crack formation mechanisms of materials from a microscopic mechanical perspective, facilitating the handling of discontinuous medium mechanics problems. In this study, the PFC3D software is utilized, and a numerical model is established based on the particle cluster modeling method using the Delaunay triangulation algorithm for grain classification. The specific process is as follows: Grain generation within the rock area based on the Delaunay triangulation algorithm. Division of the rock area into numerous sub-areas based on the boundaries of the grains. Export of each sub-area in the form of a geometric grid, followed by deletion of the original grains and sub-area partitions. Refilling of the entire rock area with small particles, which are grouped according to the exported geometric grid, thereby forming equivalent crystalline particle clusters.

**Table. 3 Microscale Mechanical Parameters of Rocks**

Meso-mechanical parameters		Numeric value (mean± mean square)
contact	Particle-particle	Linear parallel bonding model
	Particle-wall	Linear model
particle	density /(kg·m-3)	2650
	radius /(mm)	1~1.5
	Equivalent modulus /GPa	27
	Normal and tangential stiffness ratios	2
	coefficient of friction	Intra-granular	0.52
		Inter-granular	0.44
bonding	Equivalent modulus /GPa	27
	Normal and tangential stiffness ratios	2
	tensile strength /MPa	Intra-granular	110±3
		Inter-granular	36±1
	Cohesion /MPa	Intra-granular	110±3
		Inter-granular	60±2
Grain	radius /(mm)	3~4.5

To ensure that the constructed particle cluster rock model presents macroscopic physical properties like actual rocks, the key lies in calibrating the microscopic mechanical contact parameters between intra-granular and inter-granular particles (Wu et al. 2024). First, the rock model is established using the particle cluster method described above, and then numerical simulation studies of uniaxial compression and Brazilian splitting are conducted. Through repeated experiments and adjustments of model parameters, i.e., trial and error, the macroscopic physical characteristics of the simulated rock model are made to match those of actual rock specimens in the laboratory. The microscopic mechanical parameters of the rock determined by simulation calculations are shown in Table 3. Based on these parameters, the macroscopic physical characteristic parameters obtained from the simulation experiments are shown in Table 4. The simulation and experimental results of uniaxial compression and Brazilian splitting are depicted in Figure 9. The relative errors of the Poisson's ratio, elastic modulus, uniaxial compressive strength, and Brazilian splitting strength between the model and experiment are all within 5%. The uniaxial compression model approximates longitudinal fracture, while the Brazilian splitting model shows central splitting. The stress-strain curves of uniaxial compression simulation and experiment are highly similar. These results

indicate that the particle cluster DEM method used in this study can accurately construct three-dimensional rock material models, thereby ensuring the accuracy of the rock-breaking simulation by the cutterhead.

Table. 4 Macroscopic Physical Properties of Rocks

Parameters	Poisson's ratio	Elastic modulus /GPa	Tensile strength /MPa	Compressive strength /MPa
Simulation	0.33	39.99	21.87	233.85
Test	0.32	39.96	20.96	234.56
Error/%	3.13	0.07	4.34	0.30
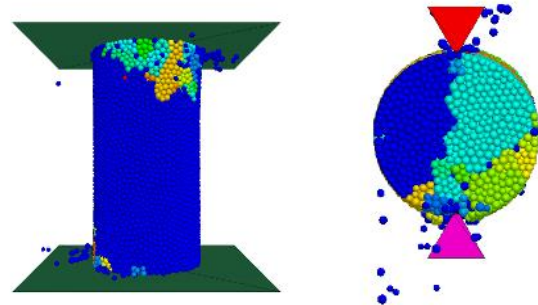
(a) Uniaxial compression and brazilian cleavage simulations
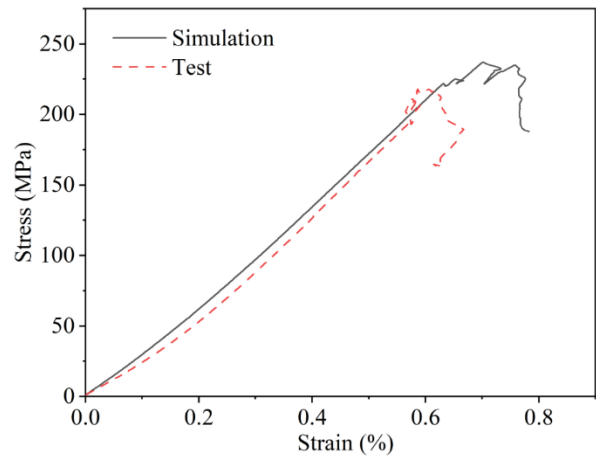
(b) Axial stress-strain curves for uniaxial compression simulations and tests

Fig. 9 Simulation and test results of uniaxial compression and brazilian splitting

4.2 Numerical simulation of rock breaking with a disc cutter

To save computational costs, the rock-breaking model adopts the full-scale sequential linear rock-breaking form with two-disc cutters, as illustrated in Figure 10. Each disc cutter has a diameter of 483 mm and a blade width of 19 mm. The initial positions of the two-disc cutters in the cutting direction are 100 mm apart, with a spacing between the cutters set at 80 mm. Considering that the cutter rings are made of alloy steel with high rigidity and strength, a rigid wall is used to simulate the cutter rings. The cutting line speed of the disc cutters is set to 0.4 m/s, and the rotational angular velocity is set to 1.65 rad/s. The dimensions of the rock model are 200 mm (length) × 250 mm (width) × 60 mm (thickness). According to the rock material modeling method described in Section 3.1, the total number of particles is approximately 272,200.
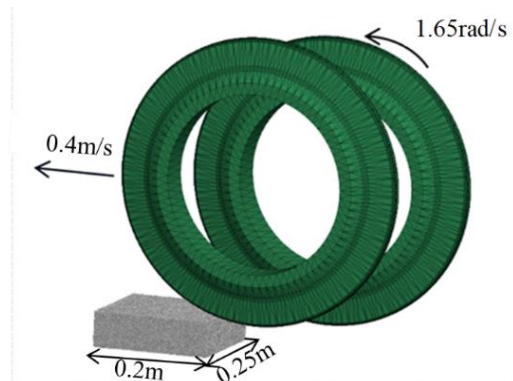

Fig. 10 Rock-breaking model with disc cutter

4.3 Analysis of the rock-breaking effect of the disc cutter

Taking the model with a penetration depth of 4 mm as an example, let's analyze the rock-breaking effect of the disc cutters. The rock debris resulting from the disc cutter rock-breaking is shown in Figure 11. In the figure, the gray particles represent the rock sample, while particles of other colors represent the rock debris generated by the rock breaking. As shown in the figure, the area directly under the cutter is a completely broken and densely compacted core area, showing an overall downward compression trend. The distribution of cracks under the cutter is shown in Figure 12. The cracks under the disc cutter extend more extensively in the lateral direction than in the vertical direction. Moreover, the cracks between the disc cutters are mainly tensile. In finite element simulations of disc cutter rock-breaking, directly removing the elements under the cutter can lead to problems such as over-breaking under the cutter and under-breaking between cutters. However, the three-dimensional discrete element method for disc cutter rock-breaking models can effectively avoid this issue.

The normal force and rolling force of the disc cutter rock-breaking are shown in Figure 13. Both the normal force and rolling force of the disc cutter exhibit a saw-toothed waveform variation. When the disc cutter cutting distance is small (l < 0.05 m) or when it is about to leave the rock mass (l > 0.175 m), due to the boundary effect, the rock fragmentation is rapid, the cutting force transmission disappears, and the overall cutting force is relatively small. When the cutting distance exceeds 0.05 m, the disc cutter enters a stable rock-breaking stage, and the cutting force gradually increases. After the rock is broken, the cutting force quickly drops to a small value, and the above-mentioned stepwise rock-breaking process is repeated.
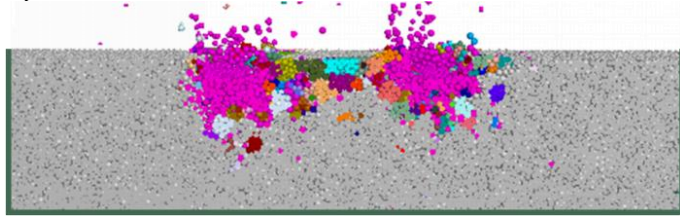

Fig. 11 The disc cutter breaks the rock ballast
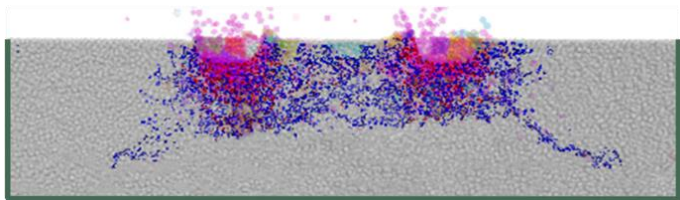

Fig. 12 Disc cutter rock-breaking crack generation and propagation

4.4 Analysis of the influence of penetration on rock breaking efficiency

For the rock-breaking simulation, disc cutters with penetration depths of 1 mm, 2.5 mm, 4 mm, 5.5 mm, 7 mm, 8.5 mm, and 10 mm were used. Seven sets of disc cutter rock-breaking simulations were conducted for each penetration depth. The triaxial forces during the rock-breaking process were recorded, and the volume of the broken rocks after completion of rock-breaking was exported. The data was organized and calculated as shown in Table 6. The relationship between the average normal force and penetration depth is shown in Figure 14.
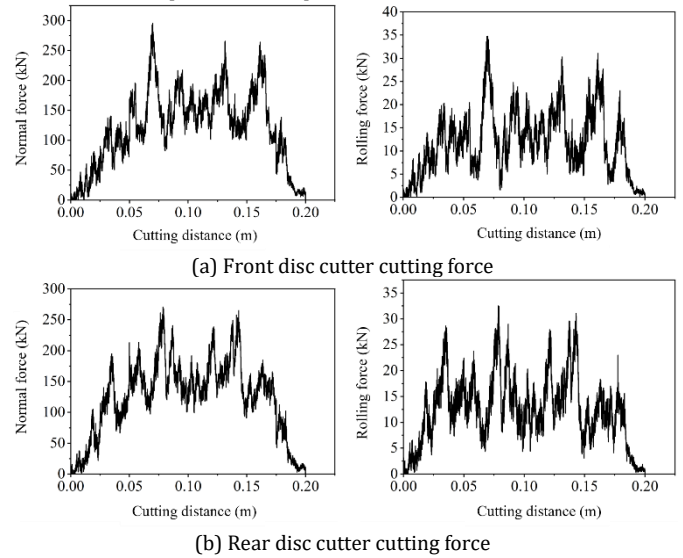

(a) Front disc cutter cutting force

(b) Rear disc cutter cutting force

Fig. 13 Cutting force of disc cutter for rock-breaking at 4mm penetration depth
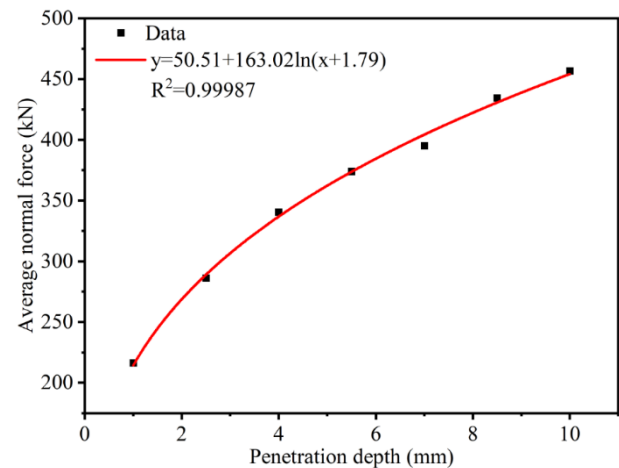

Fig. 14 Curve of the relationship between average normal force and penetration depth

Both the numerical simulation results and the experimental data of the normal force on the disc cutter during rock breaking show that as the penetration depth increases, the average normal force also gradually increases. However, the slope of the regression curve for both decreases gradually. When the penetration depth exceeds 4 mm, the rate of increase in the average normal force slows down. This indicates that even with a small increase in the average normal force, the penetration depth can increase significantly.

Based on the numerical simulation results curve shown in Figure 15, the trend of specific energy (SE) at different penetration depths can be observed. The specific energy shows an initial increase followed by a decrease with increasing penetration depth. The minimum specific energy occurs at a penetration depth of 4 mm, indicating the highest cutting efficiency at this point.

Table. 5 Summary of Simulation Results

| Penetration	Average normal force /kN		Average rolling force /kN		Cutting factor / (%)		Energy/J		Specific energy /(MJ/m³)
	Front disc cutter	Rear disc cutter	Front disc cutter	Rear disc cutter	Front disc cutter	Rear disc cutter	Front disc cutter	Rear disc cutter	
1mm	106.2	110.4	6.57	7.08	6.19	6.41	1239.79	1275.16	152.42
2.5mm	141.9	144.2	9.19	9.75	6.48	6.76	1699.06	1873.47	85.06
4mm	169.9	170.7	12.62	12.56	7.43	7.36	2306.92	2410.67	67.39
5.5mm	186.2	187.9	13.63	13.32	7.32	7.09	2589.44	2635.39	72.59
7mm	203.6	191.5	19.15	17.12	9.41	8.94	3417.48	3232.21	85.12
8.5mm	219.4	215.2	23.9	23.5	10.89	10.92	4608.20	4210.79	110.24
10mm	230.1	226.6	30.24	29.24	13.14	12.90	5337.13	5222.45	128.04
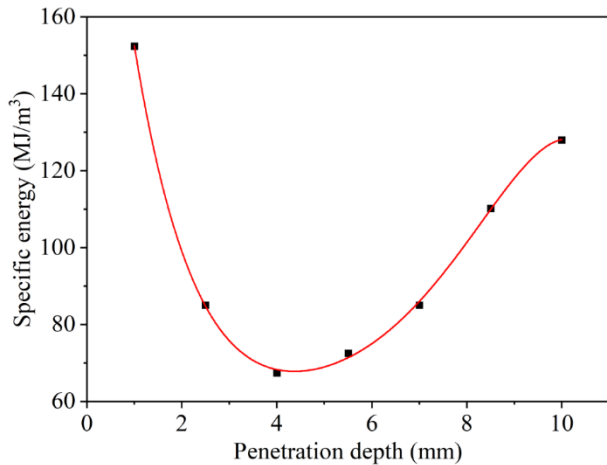
Fig. 15 Curve of the relationship between specific energy and penetration depth

In reference (Gertsch et al. 2007), the granite used in the disc cutter rock-breaking experiment had a uniaxial compressive strength of 158 MPa, tensile strength of 6.78 MPa, elastic modulus of 41.0 GPa, and Poisson's ratio of 0.234. The cutter spacing used in this study is 80 mm, which is very close to the 76 mm cutter spacing used in the experiment. By comparing the two sets of experimental data, it can be observed that under the same cutter spacing conditions, the average normal force in both experiments increases with the increase of penetration depth. However, at the same penetration depth, the average normal force obtained in this study is slightly higher. This is because the uniaxial compressive strength of the gabbro used in this study is 234.56 MPa, with a tensile strength of 20.96 MPa, which is higher than that of granite. The experimental trend of specific energy with the ratio of cutter spacing to penetration depth in reference (Cho et al. 2013) decreases first, then increases, which is like the experimental trend observed in this study.

5. Conclusion

Based on indoor disc cutter rock breaking experiments, this study used the discrete element method with particle clusters to establish a high-precision numerical model of disc cutter rock breaking. The investigation focused on the variation of disc cutter rock breaking efficiency with penetration depth and concluded:

1. The small-scale disc cutter linear rock breaking experiments and three-dimensional particle cluster disc cutter rock breaking numerical simulation models effectively reflected the real physical process of disc cutter rock breaking, providing a valuable tool for studying TBM disc cutter rock breaking mechanisms.

2. For the extremely hard gabbro studied in this paper, rock-breaking experiments under constrained conditions revealed a transition in the rock-breaking state under the cutter from squeezing to crushing as the penetration depth increased. Under unconstrained conditions, the rock mainly broke through lateral spalling. As the penetration depth increased, the amount of rock debris significantly increased, and the ejected rock debris traveled farther.

3. Rock-breaking experiments demonstrated that the normal force of the cutter was approximately linearly related to the penetration depth, increasing with the penetration depth. However, numerical simulations revealed a logarithmic relationship between the normal force of the cutter and penetration depth. The rate of increase decreased as the penetration depth increased. There exists a critical penetration depth, beyond which the increase in rock breaking load is slow, while the penetration depth significantly increases. This critical penetration depth is determined to be 4 mm.

4. Rock-breaking experiments showed that the specific energy gradually decreased with the increase in penetration depth, with the highest rock-breaking efficiency occurring at a penetration depth of 3 mm. However, simulation results indicated that the specific energy first decreased and then increased with the increase in penetration depth, with the highest rock-breaking efficiency occurring at a penetration depth of 4 mm. This discrepancy arises from the maximum penetration depth limitation of 3 mm in the small-scale experimental platform due to size and stiffness constraints. Combining the experimental and simulation results, the optimal penetration depth is suggested to be 4 mm.

Conflicts of interest

The authors declare that there are no conflicts of interest regarding the publication of this paper.

References

Cheng, Y.L. 2017. Numerical simulation of optimal penetration depth for TBM disc cutter rock breaking. Journal of Central South University (Natural Science), 48(4): 936-943. (in Chinese) https://doi.org/10.11817/j.issn.1672-7207.2017.04.012

Cho, J.W., Jeon, S., Jeong, H.Y., Chang, S.H. 2013. Evaluation of cutting efficiency during TBM disc cutter excavation within a Korean granitic rock using linear-cutting-machine testing and photogrammetric measurement. Tunnelling and Underground Space Technology, 35(4): 37-54. https://doi.org/10.1016/j.tust.2012.08.006

Fu, Y.S. 2024. Study on rock fracture characteristics and rock breaking efficiency under the action of TBM disc cutter rolling invasion. Shandong University. (in Chinese) https://doi.org/10.27272/d.cnki.gshdu.2023.001951

Geng, Q., Shi, M.L., Liu, X.Y., Lu, Y.F., Zhang, J.J., Ye, M. 2022b. Tunnel boring machine (TBM) cutter spacing design based on simulations of rock breaking process using a FEM-SPH coupling method. International Conference on Mechanical Design. Singapore: Springer. https://doi.org/10.1007/978-981-16-7381-8_136

Geng, Q., Zhang, J.J., Wang, K., Lu, Y.F., Xie, L.Y., Ye, M. 2022a. Simulation and experimental study of TBM disc cutter cutting based on FEM-SPH coupling. Journal of Shandong University (Engineering Science)，52(1): 93-102. (in Chinese)

Gertsch, R., Gertsch, L., Rostami, J. 2007. Disc cutting tests in Colorado red granite: implications for TBM performance prediction. International Journal of Rock Mechanics and Mining Sciences, 44(2): 238-246. https://doi.org/10.1016/j.ijrmms.2006.07.007

Gong, Q.M., He, G.W., Zhao, X.B., Ma, H.S., Li, X.Z., Zhang, H., Miao, C.T. 2015. Experimental study on the influence of disc cutter spacing on rock breaking efficiency of tunnel boring machine in Beishan granite. Chinese Journal of Rock Mechanics and Engineering, 37(01): 54-60. (in Chinese) https://doi.org/10.11779/CJGE201501005

Gong, Q.M., He, G.W., Zhao, X.B., Zhang, H., Miao, C.T., Yao, X.H., Liao, X.Z. 2016. Influence of different penetration degrees on rock breaking efficiency of tunnel boring machine disc cutter. Modern Tunneling Technology, 53(01): 62-68. (in Chinese) https://doi.org/10.13807/j.cnki.mtt.2016.01.010

Ji, G.D., Fu B.Y., Zhang, H.J., Geng, Q., Wang, L.C., Wang, C.L., Hu, H.Q. 2023. Research on the influence law of penetration depth of TBM disc cutters on rock breaking efficiency. Journal of Railway Science and Engineering，20(12): 4755-68. (in Chinese) https://doi.org/10.19713/j.cnki.43-1423/u.T20230089

Kou, S.Q., Lindqvist, P.A., Tang, C.A., Xu, X.H. 1999. Numerical simulation of the cutting of inhomogeneous rocks. International Journal of Rock Mechanics and Mining Sciences, 36(5): 711-717. https://doi.org/10.1016/S0148-9062(99)00039-X

Li, B., Zhang, B., Hu, M.M., Liu, B., Cao, W.Z., Xu, B. 2022. Full-scale linear cutting tests to study the influence of pre-groove depth on rock-cutting performance by TBM disc cutter. Tunnelling and Underground Space Technology, 122: 104366. https://doi.org/10.1016/j.tust.2022.104366

Liu, H.Y., Kou, S.Q., Lindqvist, P.A., Tang, C.A. 2002. Numerical simulation of the rock fragmentation process induced by indenters. International Journal of Rock Mechanics and Mining Sciences, 39(4): 491-505. https://doi.org/10.1016/S1365-1609(02)00043-6

Rostami, J., Ozdemir, L., Nilsion, B. 1996. Comparison between CSM and NTH hard rock TBM performance prediction models. Proceedings of Annual Technical Meeting of the Institute of Shaft Drilling Technology, Las Vegas, NV, USA: Institute of Shaft Drilling Technology.

Snowdon, R.A., Ryley, M.D., Temporal, J. 1982. A study of disc cutting in selected British rocks. International Journal of Rock Mechanics & Mining Sciences & Geomechanics Abstracts, 19(3): 107-121. https://doi.org/10.1016/0148-9062(82)91151-2

Su, LJ., Sun, JS., Lu, W.B. 2009. Numerical simulation study on rock breaking process of TBM disc cutter based on particle flow model. Rock and Soil Mechanics, 30(9): 2823-2829. (in Chinese) https://doi.org/10.16285/j.rsm.2009.09.050.

Tan, Q., Xu, Z.J., Xia, Y.M., Zhang, K. 2012a. Numerical study on rock breaking mechanism of TBM cutters under two cutting sequences. Journal

of Central South University: Science and Technology, 43(3): 940-946. (in Chinese)

Tan, Q., Yi, N.E., Xia, Y.M., Xu, Z.J., Zhu Y., Song J.H. 2012b. Study on dynamic characteristics of TBM disc cutter rock breaking and optimal cutter spacing. Chinese Journal of Rock Mechanics and Engineering, 31(12): 2453-2464. (in Chinese)

Tan, Q., Zhang, K., Zhou, Z.L., Xia, Y.M. 2010. Numerical simulation and experimental observation of rock fracture under spherical tooth roller cutter action. Chinese Journal of Rock Mechanics and Engineering, 29(1): 163-169. (in Chinese)

Tarasov, B., Potvin, Y. 2013. Universal criteria for rock brittleness estimation under triaxial compression. International Journal of Rock Mechanics and Mining Sciences，59: 57-69. https://doi.org/10.1016/j.ijrmms.2012.12.011

Wang, Z.Q., Wang, J.Y., Zhang, Z.M., Guan, Z.H. 2014. Experimental study on influencing factors of disc cutter rock breaking force. Journal of Northeastern University (Natural Science), 35(7): 1015-1018. (in Chinese)

Wu, W.R. 2023. Study on rock breaking mechanism and efficiency of TBM disc cutter based on the parallel bond model. Qingdao University of Science and Technology. (in Chinese) https://doi.org/10.27263/d.cnki.gqudc.2022.000650

Xia, Y.M., Guo, B., Tan, Q., Zhang, X.H., Lan, H., Ji, Z.Y. 2018. Comparisons between experimental and semi-theoretical cutting forces of CCS disc cutters. Rock Mechanics and Rock Engineering, 51(5): 1583-1597. https://doi.org/10.1007/s00603-018-1400-x

Zhang, Z.H., Liang, Z.Z., Tang, C.A., Kishida, K. 2023. A comparative study of current methods for determining stress thresholds of rock subjected to compression. Rock Mechanics and Rock Engineering, 56(11): 7795-7818. https://doi.org/10.1007/s00603-023-03480-3